Advanced Target Tracking for Applications in Multistatic Systems

Wolfgang Koch

FGAN-FKIE
Neuenahrer Strasse 20
D 53343 Wachtberg, Germany
Tel +49 228 9435 373
Fax +49 228 9435 685

email w.koch@fgan.de

Abstract

A particularly exciting topic of recent research is advanced distributed signal and data fusion for passive radar systems, where radio, TV, or mobile phone base stations are used as sources for illuminating targets of interest. Even in remote regions of the world, each transmitter of electromagnetic radiation becomes a potential radar transmitter station, which enables air surveillance by passively receiving reflections of non-cooperatively emitted signals of opportunity. In this way, the reconnaissance process remains covert and is not revealed by actively transmitting radiation. Analogous considerations are valid for sub-sea surveillance.

Digital Audio/Video Broadcasting (DAB/DVB-T) is already available in a large area of Europe. The advantage of using these signals for passive air surveillance is the disposability of a large range of illuminators sending an easily decodeable digital broadcast signal. In the considered multi-static scenario, one observer provides bistatic Time Difference of Arrival (TDoA) and Doppler measurements. The main task for target tracking is to handle ghosts that arise due to problems of association between illuminators, targets and measurements. In this paper, an approach for track initialization in a single frequency network (SFN) is discussed, which is based on clustering. Special attention will be paid to the 2D estimation performance, related to fusing TDoA measurements of two distinct illuminators. Numerical results will include performance analysis via Monte-Carlo simulations for 2D Cartesian estimation performance and an analysis of the number of reasonable estimates in a real configuration of DAB illuminators.

Detection of moving targets in stationary clutter can be accomplished by STAP radar. In contrast to monostatic radar the performance of bistatic STAP depends strongly on the actual radar-target geometry. Even for sidelooking radar the clutter Doppler is generally range dependent which causes special problems in estimating the space-time clutter covariance matrix. For certain bistatic constellations clutter notches as appearing during track (i.e. areas of low probability of detection) may be considerably wider than in monostatic radar. The bistatic transmitter-receiver constellation has strong implications on ground moving target tracking, which is basic for producing a recognized ground picture as well as for analyzing traffic flows, identifying sources and sinks of traffic, or detecting lines of communication. Aspects of a bistatic GMTI tracking algorithm are described and some typical tracking results are given. Special emphasis is placed on a suitable modeling of the bistatic radar characteristics within the tracker.

Contents

1 Introduction

By exploiting illumination by stationary or mobile transmitters of radiation, which are spatially separated from receiver stations operating cooperatively or non-cooperatively, even those objects can be passively located and tracked that are not actively transmitting radiation themselves. In this case of bistatic illumination, the reconnaissance process remains covert. In practically relevant bistatic scenarios, illuminators of opportunity like radio or television [1, 2] are of particular importance. Since the illuminators are dislocated from the receiver, instead of measuring the round trip time (RTT), we measure the Time Difference of Arrival (TDoA) between the signal received directly from the sender and delayed copies reflected of potential targets. In our application, also Doppler shift, i.e. range-rate, is measured, which gives us information about the velocity.

Using signals emitted by radio and television antennas provide interesting opportunities for passive air surveillance. We consider a network of television or radio antennas, broadcasting digital signals (DAB/DVB-T)[3] at the same frequency, a so-called single frequency networks (SFN). So, even if we consider only a single receiver, we usually obtain multiple copies, depending on the number of illuminators within range. Advantages in comparison to active systems are:

1. a saving of costs, since no additional illuminators are needed; and
2. the possibility of covert air surveillance.

Besides all these perspectives, using non-cooperative illuminators for air surveillance still holds challenges in the fields of signal processing [4] and target tracking.

In this contribution, we point out difficulties concerning target tracking and present an approach that is adapted to the special requirements of DAB and DVB-T networks. The main difficulty with respect to target tracking is that the association between illuminators and measurement is principally unknown. This leads to challenging association problems. We base our tracking algorithm on Multi Hypothesis Tracking (MHT)[5]. To decrease computational complexity we divide it into several tracking stages: The first tracking stage works directly on the incoming measurements in bistatic range and range-rate. In the second stage we generate possible 2D estimates by combining information of two illuminators and solve the association problem (Deghosting). Finding a probable 2D Cartesian target estimate is based on clustering and depends on an appropriate description of the probability density [6]. Last, the third stage delivers a 3D Cartesian state estimate. We will give numerical results for the different tracking stages via Monte Carlo Runs and discuss the dependencies between them. Estimation performance will be analyzed in terms of the averaged estimation error and includes a comparison to the corresponding average trace of the covariance matrix.

Another aspect to be discussed, continues a series of papers on tracking of ground targets with STAP radar [22]-[24]. In [22] the CRB of azimuth and Doppler estimates produced by a monostatic airborne STAP radar is used to improve tracking of moving ground targets. STAP is required to detect moving targets in ground clutter. In [2,3] ground target location is carried out by adaptive monopulse radar which produces azimuth and Doppler estimates and the associated variances. In this paper some considerations on the use of STAP radar in bistatic configurations are made. While being more complex than monostatic radar, bistatic configurations may offer favorable properties such as covert receiver position and a higher target cross section in certain radar-target constellations (anti-stealth). Some details on bistatic STAP radar can be found in [25], chapter 12.

In the bistatic case the GMTI tracking algorithms which are well-developed for monostatic GMTI radar applications [1,9], have to be adapted to measurements of the bistatic range and range-rate. The resulting non-linear measurement equations have to be treated appropriately. We here consider approximations within the framework of unscented Kalman filtering (UKF) [8]. As the association between measurements and the illuminator responsible for it is known, however, the resulting tracking task is much reduced in complexity if compared to other multistatic tracking applications such as passive radar with DAB illuminators [31]. In bistatic GMTI tracking particular emphasis has to be placed on an appropriate representation of the underlying likelihood function. Among its basic constituents is the detection probability which is now a non-trivial

function of the current sensor-to-target geometry. This bistatic likelihood function is able to model series of deteriorated or missing detections until the geometry is changing again. By exploiting the sensor detection model within the likelihood function, however, information on the current location of the clutter notch explicitly enters into the tracking algorithm and improves track continuation in such situations. As a consequence, the width of the clutter notch and the minimum detectable velocity (MDV) prove to be important tracking parameters.

This work has the following structure: Section 2 gives a very brief overview of the Bayesian tracking paradigm. In section 3 we will describe the DAB/DVB-T scenario and give an overview about the challenges with regard to target tracking. In particular we will address the derivation of the multi-stage MHT algorithm and numerical results via Monte Carlo runs. Section 4 gives a short introduction of the properties of bistatic STAP radar, where the derivation of the bistatic GMTI tracking algorithm and numerical results via Monte Carlo runs will be given. Section 5 summarizes the results.

2 Bayesian Tracking Paradigm

A Bayesian tracking algorithm is an iterative updating scheme for calculating conditional probability density functions $p(\mathbf{x}_l|Z^k)$ that represent all available knowledge on the object states $\mathbf{x}_l$ at discrete instants of time t_l. The densities are explicitly conditioned by the sensor data Z^k accumulated up to some time t_k, typically the present time. Implicitly, however, they are also determined by all available context knowledge on the sensor characteristics, the dynamical object properties, the environment of the objects, topographical maps, or tactical rules governing the objects' over-all behavior.

With respect on the instant of time t_l at which estimates of the object states $\mathbf{x}_l$ are required, the related density iteration process is referred to as *prediction* ($t_l > t_k$), *filtering* ($t_l = t_k$), or *retrodiction* ($t_l < t_k$). The propagation of the probability densities involved is given by three basic update equations, which will be derived and discussed below and illustrated by examples that appear as limiting cases of the more general Bayesian approach.

2.1 Prediction

The prediction density $p(\mathbf{x}_k|Z^{k-1})$ is obtained by combining the evolution model $p(\mathbf{x}_k|\mathbf{x}_{k-1})$ with the previous filtering density $p(\mathbf{x}_{k-1}|Z^{k-1})$:

$$p(\mathbf{x}_{k-1}|Z^{k-1}) \xrightarrow[\text{constraints}]{\text{evolution model}} p(\mathbf{x}_k|Z^{k-1}) \tag{1}$$

$$p(\mathbf{x}_k|Z^{k-1}) = \int d\mathbf{x}_{k-1}\ \underbrace{p(\mathbf{x}_k|\mathbf{x}_{k-1})}_{\text{evolution model}}\ \underbrace{p(\mathbf{x}_{k-1}|Z^{k-1})}_{\text{previous filtering}}. \tag{2}$$

2.2 Filtering

The filtering density $p(\mathbf{x}_k|Z^k)$ is obtained by combining the sensor model $p(Z_k|\mathbf{x}_k)$ with the prediction density $p(\mathbf{x}_k|Z^{k-1})$ according to:

$$p(\mathbf{x}_k|Z^{k-1}) \xrightarrow[\text{sensor model}]{\text{current sensor data}} p(\mathbf{x}_k|Z^k) \tag{3}$$

$$p(\mathbf{x}_k|Z^k) = \frac{p(Z_k, m_k|\mathbf{x}_k)\ p(\mathbf{x}_k|Z^{k-1})}{\int d\mathbf{x}_k\ \underbrace{p(Z_k, m_k|\mathbf{x}_k)}_{\text{sensor model}}\ \underbrace{p(\mathbf{x}_k|Z^{k-1})}_{\text{prediction}}}. \tag{4}$$

2.3 Retrodiction

The retrodiction density $p(\mathbf{x}_l|Z^k)$ is obtained by combining the object evolution model $p(\mathbf{x}_{l+1}|\mathbf{x}_l)$ with the previous prediction and filtering densities $p(\mathbf{x}_{l+1}|Z^l)$, $p(\mathbf{x}_l|Z^l)$ according to:

$$p(\mathbf{x}_{l-1}|Z^k) \xleftarrow[\text{evolution model}]{\text{filtering, prediction}} p(\mathbf{x}_l|Z^k) \tag{5}$$

$$p(\mathbf{x}_l|Z^k) = \int d\mathbf{x}_{l+1} \frac{\overbrace{p(\mathbf{x}_{l+1}|\mathbf{x}_l)}^{\text{evolution}} \overbrace{p(\mathbf{x}_l|Z^l)}^{\text{prev. filtering}}}{\underbrace{p(\mathbf{x}_{l+1}|Z^l)}_{\text{prev. prediction}}} \underbrace{p(\mathbf{x}_{l+1}|Z^k)}_{\text{prev. retrodiction}} \tag{6}$$

Being the natural antonym of "prediction", the technical term "retrodiction" was introduced by Oliver Drummond in a series of papers [9, 10, 11]. According to his definition (*retrodiction* "The process of computing estimates of states, probability densities, or discrete probabilities for a prior time (or over a period of time) based on data up to and including some subsequent time, typically, the current time." [9, p. 255]), this term comprises not only standard smoothing, but also the concept of a retrodicted discrete probability that is analogous to a smoothed estimate in usual Kalman filtering. For this reason, the notion of "retrodiction" is general enough and adequate also for the type of algorithms proposed above. Adopting the classical standard terminology [12], we could speak of *fixed-interval* retrodiction.

2.4 The Notion of a Track

According to this paradigm, an *object track* represents all relevant knowledge on a time varying object state of interest, including its history and measures that describe the quality of this knowledge. As a technical term, 'track' is therefore either a synonym for the collection of densities $p(\mathbf{x}_l|Z^k)$, $l = 1, \ldots, k, \ldots$, or of suitably chosen parameters characterizing them, such as estimates related to appropriate risk functions and the corresponding estimation error covariance matrices.

If possible, a one-to-one association between the objects in the sensors' field of view and the produced tracks is to be established and has to be preserved as long as possible (*track continuity*). In many applications, track continuity is even more important than track accuracy. Obviously, the achievable track quality does not only depend on the performance of the underlying sensors, but also on the object properties and the operational conditions within the scenario to be observed.

In this context, the notion of *track consistency* is important, which describes the degree of compliance between the inherent measures of track quality provided by the fusion process itself and the "real" tracking errors involved. Track consistency can be verified in experiments with an established ground truth or in Monte-Carlo-simulations.

Graphical Illustration In Figure 1a the conditional probability densities $p(\mathbf{x}_{k-1}|Z^{k-1})$, $p(\mathbf{x}_k|Z^k)$, and $p(\mathbf{x}_{k+1}|Z^{k+1})$ resulting from filtering at time instants t_{k-1}, t_k, and t_{k+1} are displayed along with the predicted densities $p(\mathbf{x}_{k+2}|\mathcal{Z}^{k+1})$. While at time t_{k-1} one sensor measurement has been processed, no measurement could be associated to it at time t_k. Hence, a missing detection is assumed. Due to the lacking sensor information, the density $p(\mathbf{x}_k|\mathcal{Z}^k)$ is broadened, since object maneuvers may have occurred. This in particular implies an increased region, where data at the subsequent time t_{k+1} are expected (gates). According to this effect, at time t_{k+1} three correlating sensor measurements are to be processed leading to a multi-modal probability density function. The multiple modes reflect the ambiguity regarding the origin of the sensor data and also characterize the predicted density $p(\mathbf{x}_{k+2}|\mathcal{Z}^{k+1})$. By this, the data-driven adaptivity of the Bayesian updating scheme is indicated.

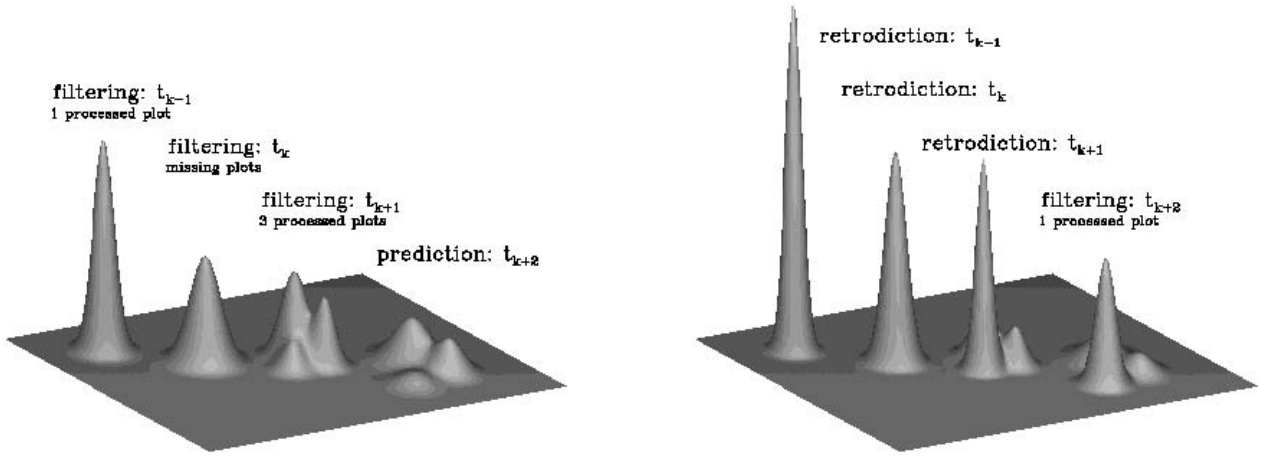

(a) Forward Iteration

(b) Backward Iteration

Figure 1: Scheme of Bayesian density iteration: conditional probability densities resulting from prediction, filtering, and retrodiction at different instants of times.

In Figure 1b, the density $p(\mathbf{x}_{k+2}|\mathcal{Z}^{k+2})$, resulting from processing a single correlating sensor measurement at time t_{t+2}, along with the retrodicted densities $p(\mathbf{x}_{k+1}|\mathcal{Z}^{k+2})$, $p(\mathbf{x}_k|\mathcal{Z}^{k+2})$, and $p(\mathbf{x}_{k-1}|\mathcal{Z}^{k+2})$ are shown. Evidently, available sensor data at the present time can significantly improve the estimates of the object states in the past.

2.5 Remarks on Approximations

Under more realistic conditions, the probability densities involved typically have the structure of finite mixtures, i.e. they can be represented by weighted sums of individual probability densities that assume particular data interpretation or model hypotheses to be true. This general structure is a direct consequence of the uncertain origin of the sensor data and/or of the uncertainty related to the underlying object evolution. In concrete implementations, however, it is always necessary to apply certain approximations in order to handle such mixtures efficiently. Provided the densities $p(\mathbf{x}_l|Z^k)$ are calculated at least approximately correctly, "good" estimators can be derived related to various risk functions adapted to the applications. What "good" means depends on the particular application considered and must often be verified by extensive Monte-Carlo-simulations and experiments.

Gaußian Mixtures At least approximately correct closed-formula solutions for the Bayesian tracking paradigm can be derived if the prediction, filtering, and retrodiction densities as well as the sensor and evolution models belong to certain families of probability densities, so-called *mutually conjugate densities*. A wide and mathematically comfortable family of conjugate densities for random vectors $\mathbf{x}$ is provided by *Gaußian Mixtues* [14], i.e. by weighted sums of Gaußian probability densities, $p(\mathbf{x}) = \sum_i p_i \mathcal{N}\big(\mathbf{x};\, \mathbf{x}_i,\, \mathbf{P}_i\big)$ with *mixture coefficients* $p_i \in \mathbb{R}$ that sum up to One, $\sum_i p_i = 1$, but need not necessarily be positive. A Gaußian mixture density is thus completely represented by a relatively small number of parameters $\{p_i, \mathbf{x}_i, \mathbf{P}_i\}_i$. As an early example see [15].

For many real-world applications, it has been shown that even more sophisticated functional relationships describing the physics of the measurement process within a sensor system can be modeled by likelihood functions of the Gaußian mixture type. Of course, the accuracy of the sensor model, i.e. the number of mixture components that are actually to be taken into account to approximately describe the underlying phenomena, depends on the requirements of the underlying application. The same arguments are valid if the

incorporation of context information, such as road maps, is to be considered or in the case of more complex dynamics models.

2.6 A Look at Track Initiation

At time t_0, the probability density $p(\mathbf{x}_0|Z^0)$ describes the initial knowledge on the object state. As an example let us consider state vectors $\mathbf{x}_k = (\mathbf{r}_k^\top, \dot{\mathbf{r}}_k^\top)^\top$, consisting of the object position and velocity, and a first position measurement $\mathbf{z}_0$ with a measurement error covariance matrices $\mathbf{R}_0$. Based on $\mathbf{z}_0$ and the context information on the maximum object speed $v_{\max}$ to be expected, a reasonable initiation is given by $p(\mathbf{x}_0|\mathbf{z}_0) = \mathcal{N}\big(\mathbf{x}_0;\, \mathbf{x}_{0|0},\, \mathbf{P}_{0|0}\big)$ with:

$$\mathbf{x}_{0|0} = (\mathbf{z}_0^\top, \mathbf{o}^\top)^\top, \quad \mathbf{P}_{0|0} = \mathrm{diag}[\mathbf{R}_0, v_{\max}^2 \mathbf{I}]. \tag{7}$$

In the case of an IMM evolution model, we consider the probability density $p(\mathbf{x}_0, i_0|Z^0) = p_{0|0}^{i_0}\, \mathcal{N}\big(\mathbf{x}_0;\, \mathbf{x}_{0|0}^{i_0},\, \mathbf{P}_{0|0}^{i_0}\big)$ with $p_{0|0}^{i_0} = \frac{1}{r}$. For a numerically robust and quick initiation scheme from even incomplete measurements see [17, 18] and the literature cited herein.

Iterative tracking algorithms must be initiated appropriately. Under simple conditions, this is not a difficult task, as has been shown above (Equation 7). For low observable objects, i.e. objects embedded in a high clutter background [5, 19, 20, 21] or in case of incomplete measurements [17, 18], more than a single set of observations at particular data collection times are usually necessary for detecting all objects of interest moving in the sensors' fields of view. Only then, the probability density iteration can be initiated based on 'extracted' object tracks, i.e. by tentative tracks, whose existence is 'detected' by a detection process working on a higher level of abstraction, which makes use of a time series of accumulated sensor data $Z^k = \{Z_i\}_{i=1}^k$.

Assuming well-separated objects at first for the sake of simplicity, we thus have to decide between two alternatives before a tracking process can be initiated:

- h_1: Besides false data, Z^k contains also real object measurements.
- h_0: There is no object existing in the FoV; all sensor data in Z^k are false.

As special case of the more general theory of statistical decision processes, the performance of a track extraction algorithm is characterized by two probabilities related to the decision errors of first and second kind:

1. $P_1 = P(\text{accept } h_1|h_1)$, i.e. the conditional probability that h_1 is accepted given h_1 is actually true (corresponding to the detection probability P_D of a sensor).
2. $P_0 = P(\text{accept } h_1|h_0)$: the conditional probability that h_1 is accepted given it is actually false (corresponding to the false alarm probability P_F of a sensor).

Sequential Likelihood Ratio Test In typical tracking applications, the decisions between the alternatives must be made as quickly as possible on average for given decision probabilities P_0, P_1. The decision algorithm discussed below fulfills this requirement and is of enormous practical importance. It is called *Sequential Likelihood Ratio Test* and was first proposed by Abraham Wald [19, 20].

The starting point for sequential decision making in the context of track extraction is the ratio of the conditional probabilities $p(h_1|Z^k)$ of h_1 being true given all data have been processed appropriately and $p(h_0|Z^k)$ of h_0 being true given the sensor data. If $p(h_1|Z^k)$ is close to One and $p(h_0|Z^k)$ close to Zero, the ratio is large, while it is small if $p(h_1|Z^k)$ is close to Zero and $p(h_0|Z^k)$ close to One. If both hypotheses are more or less equally probable, the ratio is of an intermediate size. According to Bayes' Theorem, we obtain:

$$\frac{p(h_1|Z^k)}{p(h_0|Z^k)} = \frac{p(Z^k|h_1)}{p(Z^k|h_0)}\,\frac{p(h_1)}{p(h_0)}. \tag{8}$$

Since the a priori probabilities $p(h_1)$ and $p(h_0)$ are in most applications assumed to be equal, this defines a test function, which is called *likelihood ratio*:

$$\mathrm{LR}(k) = \frac{p(Z^k|h_1)}{p(Z^k|h_0)} \tag{9}$$

and can be calculated iteratively by exploiting the underlying object evolution and sensor models $p(\mathbf{x}_k|\mathbf{x}_{k-1})$ and $p(Z_k|\mathbf{x}_k)$.

An intuitively plausible sequential test procedure starts with a time window of length $k = 1$ and iteratively calculates the test function $\mathrm{LR}(k)$ until a decision can be made. At each step of this iteration the likelihood ratio is compared with two thresholds A and B:

$$\begin{array}{lll} & \mathrm{LR}(k) < A, & \text{accept the hypothesis } h_0 \text{ (i.e. no object existent)} \\ \text{for} & \mathrm{LR}(k) > B, & \text{accept the hypothesis } h_1 \text{ (i.e. an object exists)} \\ & A < \mathrm{LR}(k) < B, & \text{expect new data } Z_{k+1}\text{, repeat the test with } \mathrm{LR}(k+1). \end{array}$$

Properties Relevant to Tracking Note that the iterative calculation of likelihood ratios has a meaning, which is completely different from the iterative calculation of probability density functions, although similar formulae and calculations are implied as will become clear below. By iteratively calculated likelihood ratio we wish to make a the *decision*, whether an iterative tacking process should be initiated or not.

1. The most important theoretical result on sequential likelihood ratio tests is the fact that the test has a *minimum decision length on average* given predefined statistical decision errors of first and second kind, which have to be specified according the the requirements in a given application.

2. Furthermore, the thresholds A, B can be expressed as functions of the decision probabilities P_0, P_1, i.e. they can be expressed as functions of the statistical decision errors of first and second kind and are thus not independent test parameters to be chosen appropriately. A useful approximation in many applications, is given by:

$$A \approx \frac{1-P_1}{1-P_0}, \quad B \approx \frac{P_1}{P_0}. \tag{10}$$

Relation to MHT Tracking Likelihood ratios $\mathrm{LR}(k)$ can be calculated iteratively as a by-product of the standard Bayesian tracking methodology previously discussed, provided we look upon it from a different perspective. This can be seen directly:

$$\mathrm{LR}(k) = \frac{p(Z^k|h_1)}{p(Z^k|h_0)} \tag{11}$$

$$= \frac{\int d\mathbf{x}_k \, p(Z_k, m_k, \mathbf{x}_k, Z^{k-1}|h_1)}{p(Z_k, m_k, Z^{k-1}, h_0)} \tag{12}$$

$$= \frac{\int d\mathbf{x}_k \, \overbrace{p(Z_k, m_k|\mathbf{x}_k, h_1)}^{\text{likelihood}} \, \overbrace{p(\mathbf{x}_k|Z^{k-1}, h_1)}^{\text{prediction}}}{\underbrace{|\mathrm{FoV}|^{-m_k} \, p_F(m_k)}_{\text{clutter model}}} \, \mathrm{LR}(k-1). \tag{13}$$

According to these considerations, the likelihood ratio is in general a sum of a temporally increasing number of individual likelihood ratios,

$$\mathrm{LR}(k) = \sum_i \lambda_k^i. \tag{14}$$

For avoiding memory explosion in calculating the likelihood ratio, the same type of mixture approximation techniques as previously discussed can be applied (merging of similar, pruning of too small summands λ_k^i). As soon as a decision in favor of object existence is taken, e.g. at time t_k, the normalized individual likelihood ratios can be used for initializing the tracking process:

$$p(\mathbf{x}_k|Z^k) = \sum_i \frac{\lambda_k^i}{\sum_j \lambda_k^j} \mathcal{N}(\mathbf{x}_k;\, \mathbf{x}_{k|k}^i,\, \mathbf{P}_{k|k}^i), \tag{15}$$

where $\mathbf{x}_{k|k}^i$ and $\mathbf{P}_{k|k}^i$ are by-products of the calculation of λ_k^i. As soon as the track has been initiated, the calculation of the likelihood ratio can be restarted as it is a by-product of track maintenance. The output of these subsequent sequential ratio tests can serve for re-confirming track existence or track deletion, depending on the test output. See [19, 5] for details. So far, the problem of multiple well-separated object track extraction, track maintenance, and track deletion, i.e. the full life cycle of a track, is solved in principle. See [21] for an alternative calculation of $\mathrm{LR}(k)$ by using PMHT techniques and [16] for a proof that for well separated objects this scheme is identical with Gaußian Mixture Cardinalized PHD filtering (GM-CPHD).

3 Multistatic Tracking using DAB/DVB-T

W.l.o.g. the passive observer will be positioned at the origin. The positions of the ith stationary illuminator is given in Cartesian coordinates by $\mathbf{x}_{s,i}$. Time Difference of Arrival (TDoA) and the bistatic Doppler shift are measured, which are directly correlated to the bistatic range r_i and bistatic range-rate $\dot{r}_i$.

$$\text{TDoA} = \frac{r_i - ||\mathbf{x}_{s,i}||}{c}, \qquad \text{Doppler} = -\frac{\dot{r}_i}{\lambda}, \tag{16}$$

where c is the speed of light and λ the wavelength of the signal. The measurement equations in bistatic range and range-rate are,

$$r_i = ||\mathbf{p}|| + ||\mathbf{p} - \mathbf{x}_{s,i}|| \qquad \dot{r}_i = \left(\frac{\mathbf{p}}{|\mathbf{p}|} + \frac{\mathbf{p} - \mathbf{x}_{s,i}}{|\mathbf{p} - \mathbf{x}_{s,i}|} \right)^T \cdot \mathbf{v}, \tag{17}$$

where $\mathbf{p}$ and $\mathbf{v}$ denote the target's position and velocity in Cartesian coordinates. The bistatic range equation describes ellipsoids in three-dimensional Cartesian space with foci at the observer and illuminator. The bistatic Doppler shift depends on the geometry and velocity of the target. With the target state $\mathbf{x} = (\mathbf{p}, \mathbf{v})^T$ and the measurement vector $\mathbf{z}_i = (r_i, \dot{r}_i)^T$, we abbreviate the measurement equation by $\mathbf{z}_i = h(\mathbf{x}, \mathbf{x}_{s,i})$.

We estimate the target position and velocity from two synchronous measurements using two different illuminators ($\mathbf{x}_{s,1}$ and $\mathbf{x}_{s,2}$). If we project this scenario on a 2D plane, geometrically, this would be intersecting two ellipses with foci at the origin and $\mathbf{x}_{s,i}$, c.f. Fig. 2. This basically means solving two quadratic equations successively, which can render up to four solutions, but since in this case the two ellipses share one focal point, there will be only two solutions. To estimate the velocity, we see that (17) is linear in $\mathbf{v}$. After the position has been estimated, if we set the speed in z to zero, two Doppler measurements give us a linear equation system. Of course if the position estimate is off, this will heavily punch through on the velocity estimate.

Estimation ambiguity adds to already existing ambiguity problems – not being able to associate measurements to senders – not to speak about multi-target tracking.

3.1 Problem Statement

To discuss the association problem, we consider the following example of one target, one observer and three illuminators, which involves up to three TDoA and Doppler measurements per time stage, see Fig. 3.

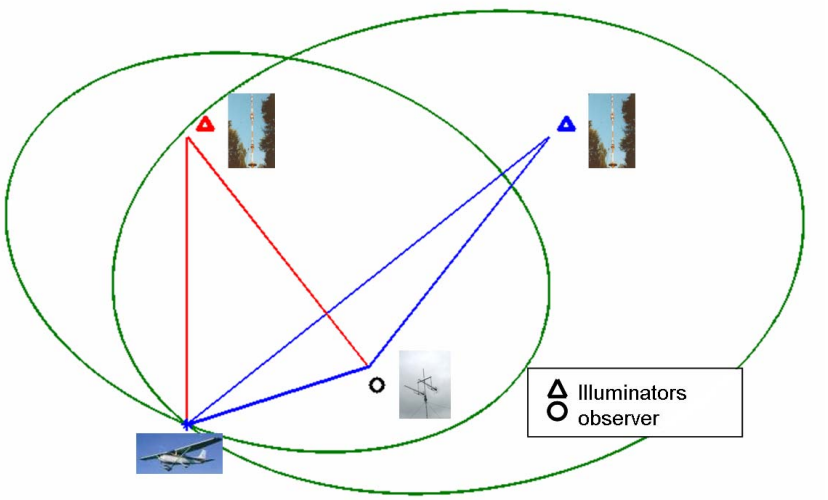

Figure 2: 2D scenario, combining TDoA information of two illuminators

Table 1: Number of target estimates

N	2	3	4	5	6
$\binom{N}{2}$	1	3	6	10	15
$\binom{N}{3}$	0	1	4	10	20

Mis-association and ambiguity result in false estimates (ghosts) that show similar movements like a target. However, good knowledge of the target movement may help to unmask some ghosts.

The approach, presented here, is based on a different criterion. We exploit that target estimates lie close to each other. So, if we regard measurements of more than two illuminators, this will result in target clustering. This method avoids fostering ghost tracks and provides a quick decision criterion. But doing so, target measurements of at least three illuminators are needed to extract a target track.

Without any error the target would lie in the intersection of all the ellipses. However, in a real scenario we have to consider noisy measurements and additional error caused by the unknown height of the object , because the third dimension is neglected in this model. Further, finding the true target will be impeded by missing detections.

Measurements of at least three illuminators are also a prerequisite for 3D Cartesian state estimation, which is of course the final aim of target tracking. For sure, combining measurements of three illuminators also yields a better 2D estimation performance, since the influence of the unknown height of the target can be neglected. Nevertheless, considering the number of possible combinations, justifies working with combinations of only two illuminators in the Deghosting stage.

In the following we define M to be the number of measurements and N the number of illuminators. Then we focus on the association problem, that arises, if 2 or 3 measurements are combined. The number of true target estimates is $\binom{N}{2}$ or $\binom{N}{3}$ respectively. For clustering to work well the number of true target estimates should be as large as possible. Combining three measurements is only favorable, if data of six illuminators is available, c.f. Table 1. Moreover, we would need at least four illuminators to solve the association problem. Besides, we have to consider the number of total possibilities, given by $2\binom{N}{2}M(M-1)$ in the 2D-case

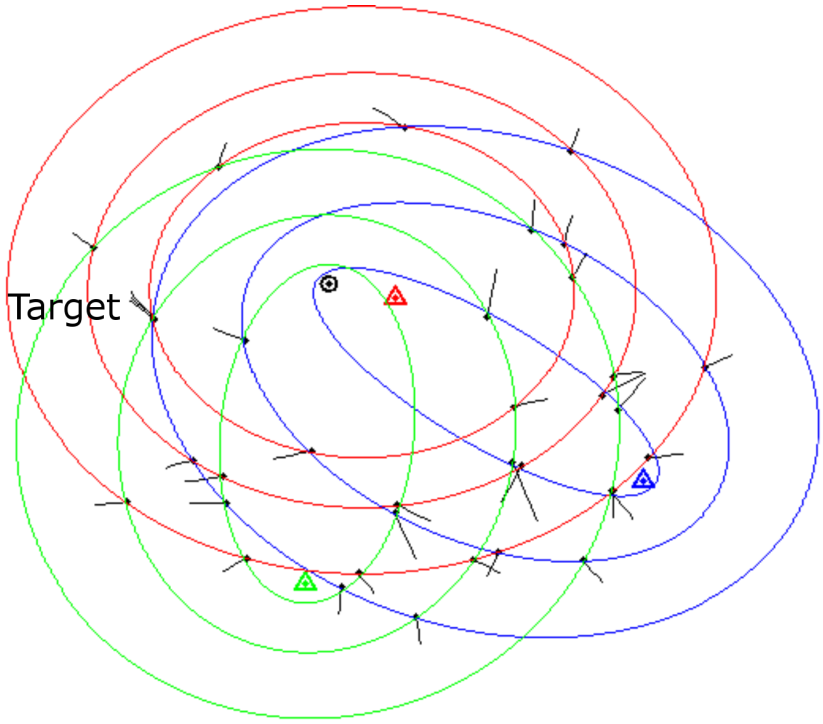

Figure 3: Association problem: one target, three illuminators (triangles), one receiver (circle), three measurements, one time scan; TDoA measurements, associated to different illuminators, are shown with ellipses; 2D estimates are given by black dots with corresponding velocity vectors

Table 2: Number of total estimates

$N = 5$, M	5	6	7	8	9	10
total:	400	600	840	1120	1140	1800
total:	600	1200	2100	3360	5040	7200

and $\binom{N}{3} M(M-1)(M-2)$[1] in the 3D case. Since the number of measurements is usually larger than the number of illuminators (multiple targets and false alarms) the 3D case would blow up complexity, c.f. Table 2

3.2 Primary Tracking of the Measured Data

To be able to distinguish between ghosts and targets we need a high probability of detection. But an increasing number of measurements will lead to increasing computational complexity. We use a primary tracking stage to select measurements of moving objects and to enhance the probability of detection. Tracking is done by Multihypothesis Tracking (MHT) [5] assuming a third order motion model. The state vector of the primary tracking stage is given by $\bar{\mathbf{z}} = (r, \dot{r}, \ddot{r})^T$, where r and $\dot{r}$ are measured and $\ddot{r}$ is initialized with zero mean. With this assumption we restrict the movements of potential tracks to reasonable behavior of range and corresponding range-rate.

[1] Combining three measurements gives usually only one solution (non-ambiguous), since the second solution can be neglected by only considering heights greater than zero.

The primary tracking stage is not only important in terms of computational speed, but is also a prerequisite to decide on association possibilities considering several time stages, since measurements collected in one track belong to the same target and illuminator.

3.3 Deghosting in Cartesian Coordinates

During the course of the algorithm, we need to destine Cartesian target state estimates. Tracking will be done again by MHT starting from a probable target state estimate. Since the request for 3D Cartesian estimates would make association more difficult, we transform measurements of two different illuminators into 2D Cartesian estimates with a fixed height. At the moment we have no knowledge about association and need to consider all possibilities. Enumerating all these possibilities in future stages would lead into memory overload fast. We therefore want to decide soon if an estimate belongs to a true target and get rid of additional ballast. Likelihood Ratio (LR) testing supplies a quick appraisal to find the true association possibilities.

For a given region G in 2D-Cartesian coordinates of volume $|G|$ we model the background distribution according to a Poisson distribution. The probability to observe n false estimates in the region G is given by

$$p_F(n) = \frac{1}{n!}(|G|\rho_F)^n e^{-|G|\rho_F}, \tag{18}$$

with spatial false return density ρ_F. Certainly, this assumption does not hold for different time stages. Moreover, since false 2D Cartesian estimates are generated by false association systematically and not randomly, we will be able to calculate the spatial false estimate density from the knowledge of observed measurements and number of considered illuminators.

3.3.1 Finding probable target estimates

Every estimate $\hat{\mathbf{x}} = (\hat{\mathbf{p}}, \hat{\mathbf{v}})$ is currently given by a position and velocity vector and a corresponding covariance matrix $\hat{\mathbf{P}}$, i.e. $\mathbf{x} \sim \mathcal{N}(\mathbf{x}; \hat{\mathbf{x}}, \hat{\mathbf{P}})$. So, for example, the true target state is supposed to lie inside the 3σ gate given by the covariance matrix with probability 0.937 [7].

For every state estimate $\hat{\mathbf{x}}$ we will count for the number of estimates $\hat{\mathbf{x}}_i$ lying in its $k\sigma$ gate, i.e.

$$n = \#\{\hat{\mathbf{x}}_i | (\hat{\mathbf{x}} - \hat{\mathbf{x}}_i)^T \hat{\mathbf{P}}^{-1} (\hat{\mathbf{x}} - \hat{\mathbf{x}}_i) < k^2\}. \tag{19}$$

We calculate a Likelihood Ratio considering the hypotheses $\mathcal{H}_0$ the true target state estimates lie inside this region and $\mathcal{H}_1$ there are only false estimates. Since the setup parameters (probability of detection (P_d), false return density ρ_F, number of illuminators N) are given in terms of measurements and not in 2D-Cartesian, we need to reconstruct the number of associated measurements m from the number of observed estimates n using the relationship $n = \binom{m}{2}$. Solving for m yields a functional relationship dependent on n:

$$m_n = \begin{cases} 0 & \text{if } n = 0 \\ \frac{1}{2} + \sqrt{\frac{1}{4} + 2n} & \text{otherwise} \end{cases} \tag{20}$$

With this, the probability of finding n estimates, including available true target estimates, can be approximated by a binomial sum depending on the probability of detection and the number of illuminators,

$$p(n|\mathcal{H}_0) = \sum_{i=0}^{n} \binom{N}{m_i} P_d^{m_i} (1 - P_d)^{N - m_i} p_F(n - i). \tag{21}$$

Here P_D is the mean probability of detection of all illuminators involved, generally it is dependent on the geometry, so using different P_Ds for different illuminators should be more reasonable in a real scenario.

The LR will be calculated by dividing the probability, that no measurement belongs to a target using the background distribution with volume vol

$$L(\hat{\mathbf{x}}) = \frac{p(n|\mathcal{H}_0)}{p_F(n)}. \tag{22}$$

In the four dimensional (2D position and 2D velocity) case the volume of the $k\sigma$ area can be calculated by [7]

$$vol = \frac{k^4\pi^2}{2}\sqrt{\det(\hat{\mathbf{P}})}. \tag{23}$$

In the following we call estimates probable, if $L(\hat{\mathbf{x}}) > 1$.

In some points this approach is heuristic, but has shown to work quite well, see subsection 3.6. To do calculation more exactly we would need to replace (19) by,

$$n = \#\{\hat{\mathbf{x}}_i|(\hat{\mathbf{x}} - \hat{\mathbf{x}}_i)^T(\hat{\mathbf{P}} + \hat{\mathbf{P}}_i)^{-1}(\hat{\mathbf{x}} - \hat{\mathbf{x}}_i) < k^2\}. \tag{24}$$

However, computational complexity increases enourmously by inverting matrices in each single step.
An alternative approach is to look back at the measurements space. For each estimate and each possible illuminator $\mathbf{x}_{s,j}$ we need to destine an expectation $\hat{\mathbf{z}}^j$ and covariance $\hat{\mathbf{R}}^j$ according to the relationship given by the measurement equation h. As an advantage the measurement covariance matrix $\mathbf{R}$ is fixed, so (19) can be replaced by

$$n = \#\{\mathbf{z}_i|(\hat{\mathbf{z}}^j - \mathbf{z}_i)^T(\hat{\mathbf{R}}^j + \mathbf{R})^{-1}(\hat{\mathbf{z}}^j - \mathbf{z}_i) < k^2\}. \tag{25}$$

Both approaches ensure that we take care of the actual uncertainty for geometrical reasons given by the covariance matrix. Regarding to estimates with big uncertainties we will need to search in a bigger region for similar estimates, simultaneously the probability to find some estimates by chance increases. Therefore, it will be important to describe the error in the covariance matrix well. Since generally the height of the object is not known in advance, we pick up uncertainties, resulting from the unknown height, in the covariance matrix [6].

3.3.2 Evaluate association possibilities

The main task of this second tracking stage is to evaluate association possibilities. In the previous subsection we derived an approach to neglect measurement to illuminator combinations by LR testing. Probable estimates, describing a possible association between measurements and illuminators for one time stage, will be used as input data of a second MHT to evaluate association. To do this, we use Likelihood Ratio testing according to the track extraction technique presented in [19].

Let $Z^T = (\mathbf{z}_{t=T_0^m}^T)$ describe a primary track in measurements up to time T, where T_0^m is the time of track extraction in measurements and $\mathbf{z}_t$ holds all information of the track at time t. If a 2D track Y^T belonging to target i is extracted, we can pursue with LR testing. Considering

$\mathcal{H}_0$: Z^T belongs to target i and illuminator j and

$\mathcal{H}_1$: Z^t belongs either not to illuminator j or target i.

we iteratively calculate

$$\begin{aligned} &p(Z^T|\mathbf{x}_{s,j}, \mathcal{H}) \\ &\quad = p(\mathbf{z}_T|Z^{T-1}, \mathbf{x}_{s,j}, \mathcal{H})p(Z^{T-1}|\mathbf{x}_{s,j}, \mathcal{H}), \end{aligned} \tag{26}$$

where $p(\mathbf{z}_T|Z^{T-1}, \mathbf{x}_{s,j}, \mathcal{H}_0)$ will be calculated during the filtering update and $p(\mathbf{z}_T|Z^{T-1}, \mathbf{x}_{s,j}, \mathcal{H}_1) = |FoV|^{-1}$, i.e. false associated measurements are supposed to be uniformly distributed in the observation area FoV. A measurement track will be allocated to a given 2D track if the LR exceeds a given threshold or will it be neglected if it undergoes one.

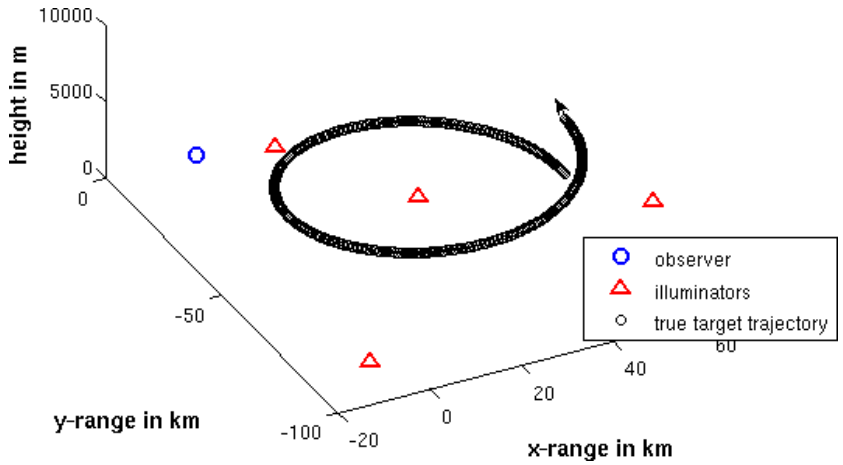

Figure 4: Simulated scenario: constellation of observer and illuminators is based on a real DAB network in Rheinland-Pfalz, Germany

3.4 3D Tracking

The final stage of the tracking algorithm yields a 3D Cartesian estimate by fusing all available information collected in the previous tracking stages. So, if information of more than two illuminators is available, it will deliver improved 2D estimates and additional information about the height of the target.

3.5 Runtime Considerations

The runtime of the MHT algorithm does mainly depend on the number of considered hypotheses. So, an increasing number of false alarms as input of the algorithm will lead to increasing computational complexity. However, in this case the second tracking stage, the Deghosting, seems to be more time consumptive than the primary tracking. The realtime-capability of the algorithm does mainly depend on how fast a decision between ghosts and targets can be reached. The more illuminators are considered, the more combinations need to be tried out, but the better association works.

3.6 Numerical Analysis

In this section we discuss numerical results for a scenario with four illuminators, one receiver and one target flying in a circle, c.f. Fig. 4. Starting with a height of 4km the target climbs slightly to 7.6km. The constellation is based on true DAB sender localizations in Rheinland-Pfalz, Germany.
The probability of detection is chosen to be 0.9 for each illuminator-receiver pair. Measurements are gathered every 10sec. with Gaussian distributed measurement error of zero mean. The measurement covariance matrix of the bistatic range and range-rate is given by $\mathbf{R} = \mathrm{diag}[](\sigma_r^2, \sigma_{\dot{r}}^2)$ with $\sigma_r = 65m$ and $\sigma_{\dot{r}} = 2m/s$. The false alarm rate is 20 false measurements per time stage and is uniformly distributed in the measurement space. To generate 2D Cartesian estimates we use the following modeling assumptions on the target height: $z \sim \mathcal{N}(5\mathrm{km}, 2\mathrm{km})$.

In Fig. 5 the results of the primary tracking stage are shown. Four measurement tracks are extracted, one track for each illuminator. We note that modeling movements in bistatic range and range-rate is difficult, since movements depend on the unknown target-illuminator-receiver geometry. For example the track colored in magenta shows a hard turn, when the target crosses the associated illuminator.

For a statistical analysis we use 100 Monte Carlo Runs and compare the root-mean-squared error (RMSE) with the root-mean trace of the covariance (RMTC), i.e. for the estimates $\hat{\mathbf{x}}_i$, truth $\mathbf{x}$ and estimated covariance

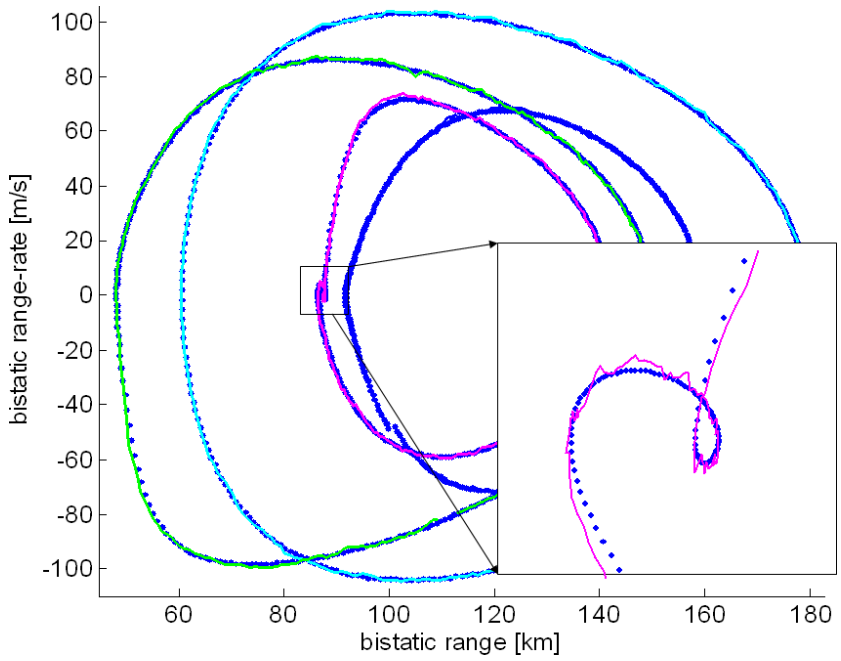

Figure 5: Primary tracking: tracking results for different iluminator-receiver pairs are shown by different colors; true measurements (without error) are plotted by blue dots.

$\hat{\mathbf{P}}_i$

$$\begin{aligned} \text{RMSE}(\mathbf{x}) &= \sqrt{\frac{1}{N}\sum_{i=1}^{N} |\hat{\mathbf{x}}_i - \mathbf{x}|^2} \\ \text{RMTC}(\mathbf{x}) &= \sqrt{\frac{1}{N}\sum_{i=1}^{N} \text{trace}(\hat{\mathbf{P}}_i)}. \end{aligned} \tag{27}$$

In Fig. 6 the RMSEs of the strongest hypothesis are plotted for each illuminator-receiver pair in different colors; for comparison the RMTC is added in black. Due to maneuverings the results are not persistently consistent, during the critical phases the RMSE increases faster than the RMTC.

Fig. 7 responds to the second tracking stage, the Deghosting in 2D Cartesian. We compare the RMSE of the x/y position estimate with the corresponding RMTC. The RMSE is sligthly increasing whilst the RMTC has nearly the same level during the whole run. This could be explained by the target height. The RMSE increases the more the actual height of the target differs from the expected height (here: 5km). In contrast, the RMTC does not depend on the actual height but only on the modeling assumptions. So, if the target height exceeds a certain value, dependent on the assumed deviation (here: 2km), tracking fails.

The information accumulated in previous tracking stages will next be transformed into 3D Cartesian estimates. The 3D Tracking depends directly on the Deghosting stage and the primary tracking and can not be analyzed separately. In Fig. 8 the mean number of measurements, which could be allocated to the track, is plotted against time. The estimation performance in height, delivered by the 3D tracking, is directly correlated to the number of measurements used; the RMSE is shown in Fig. 9. Availability of four instead of only three measurements results in improved height estimation. Fig. (10) shows numerical results for the 3D tracking performance in x/y. Again, the RMSE in x/y-position is compared to the RMTC. We observe a better estimation performance, compared with the 2D tracking stage, if measurements of three or four illuminators can be fused. On the other hand the estimation performance is strongly influenced by the allocation of measurements that is done in the Deghosting stage and depends therefore on the geometry and

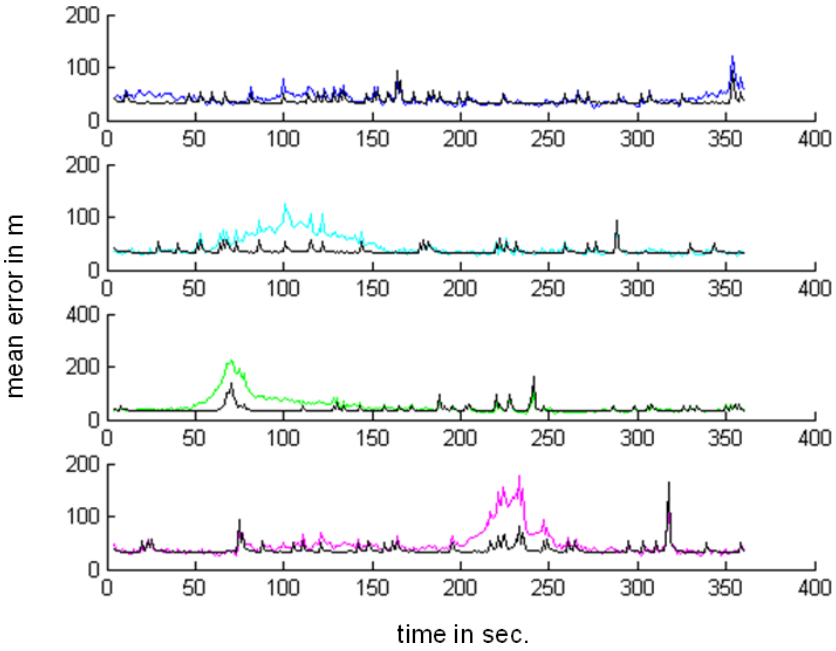

Figure 6: Primary tracking: RMSE of different illuminator-receiver pairs is shown by different colors; RMTC in black

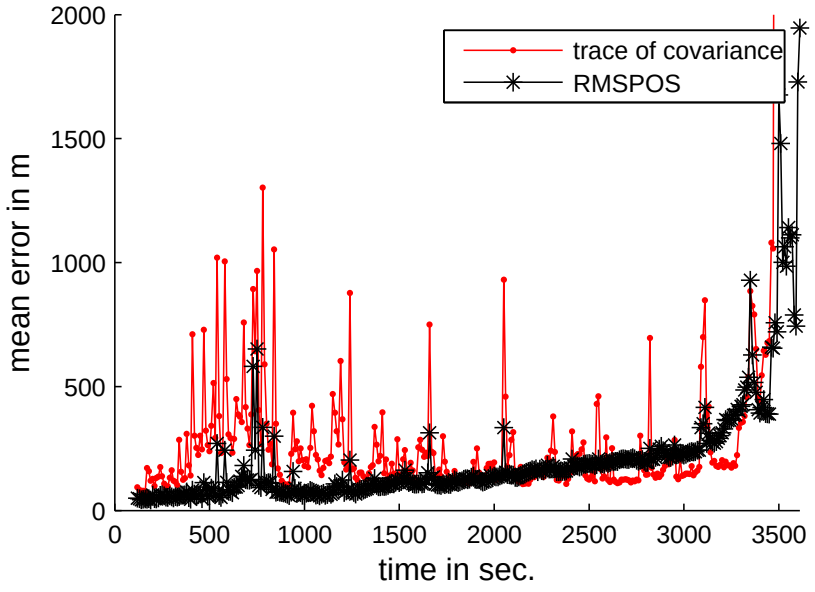

Figure 7: 2D Cartesian Tracking: RMSE and RMTC in x/y

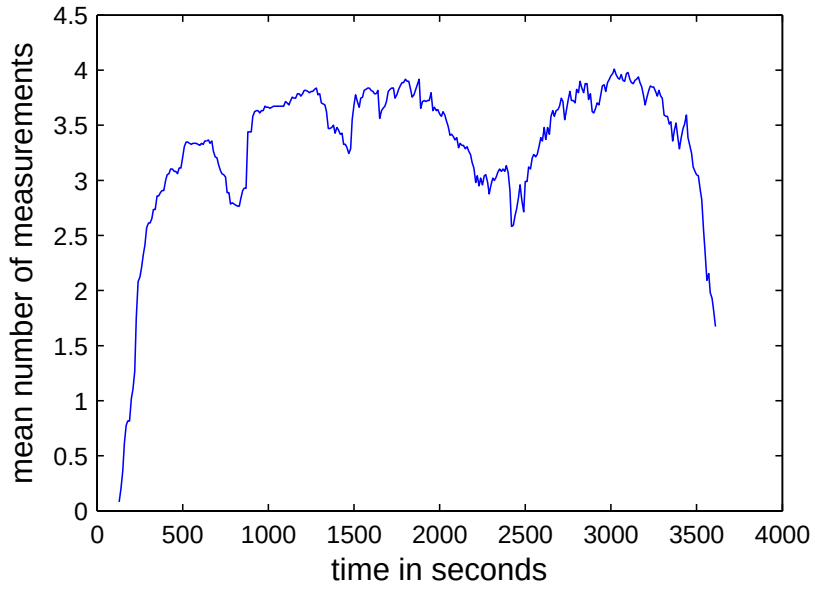

Figure 8: Mean number of measurements that could be allocated to the 2D track for each scan.

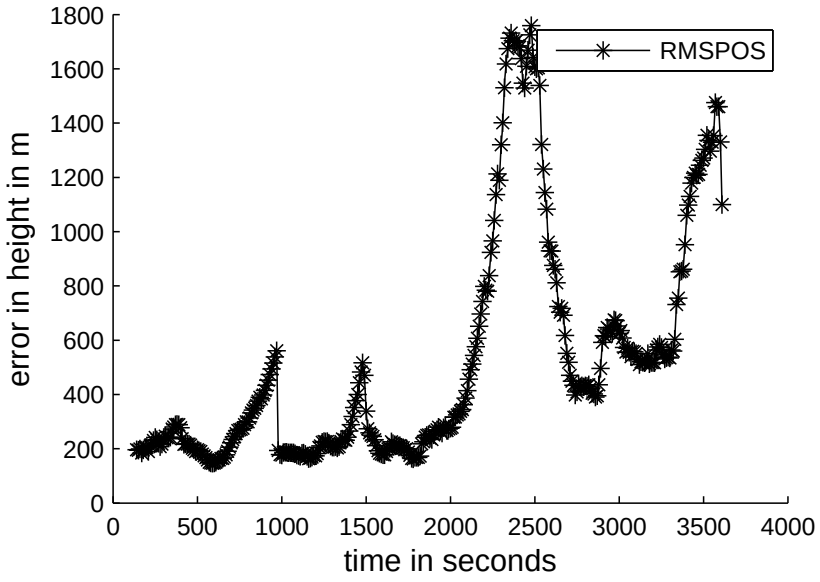

Figure 9: RMSE of target height for 3D Cartesian Tracking

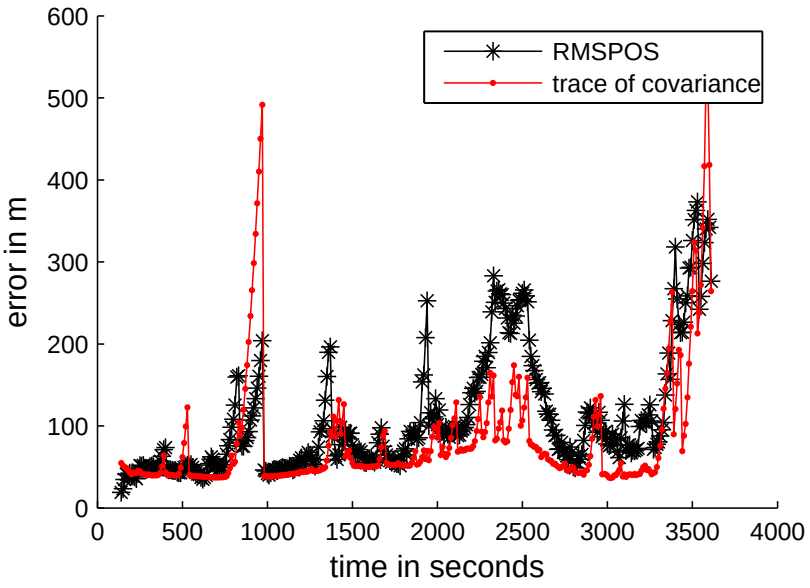

Figure 10: 3D Tracking results: RMSE and RMTC in x/y

on a good appraisal for the height of the object. At the end of the flight the target exceeds the height of 7km and association fails.

Number of probable estimates In this subsection we discuss the dependency of the approach on the target-illuminator-receiver geometry. We consider the same scenario as described above, but set $P_D = 1$ and do not consider false measurements. We will run 100 Monte-Carlo simulations in a plane of 150km by 140km (possible target positions, velocity is chosen randomly) considering the number of probable estimates, which are selected by Likelihood Ratio testing, see subsection 3.3.1.

Fig. 11 shows the mean number of true target estimates (maximal 6) that could be found by LR testing for each geometry. In a region close to the receiver finding probable target estimates is difficult due to bad geometrical conditions (estimates with covariance greater than 1.5km are ignored), but there are also large areas, where the number is greater than one, which is sufficient for 2D tracking. Considering all possible combinations (here: 144), we are also interested in the number of ghost estimates that are declared to be probable erroneously. For these simulations the maximal mean number is 9, which is a low false alarm rate for the MHT.

4 Tracking of ground targets with bistatic airborne radar

4.1 Properties of bistatic STAP radar

In the following we focus on two important properties of bistatic STAP radar: the dependence of the clutter Doppler on range and the distribution of clutter Doppler frequencies on the ground. The clutter Doppler frequency is given by

$$f_D = \frac{\nu_T}{\lambda}\cos(\varphi_T - \delta_T)\cos\vartheta_T + \frac{\nu_R}{\lambda}\cos(\varphi_R - \delta_R)\cos\vartheta_R \tag{28}$$

where ν means velocity, φ azimuth, ϑ elevation, δ course angle and λ wavelength. The subscripts R and T refer to receiver and transmitter, respectively.

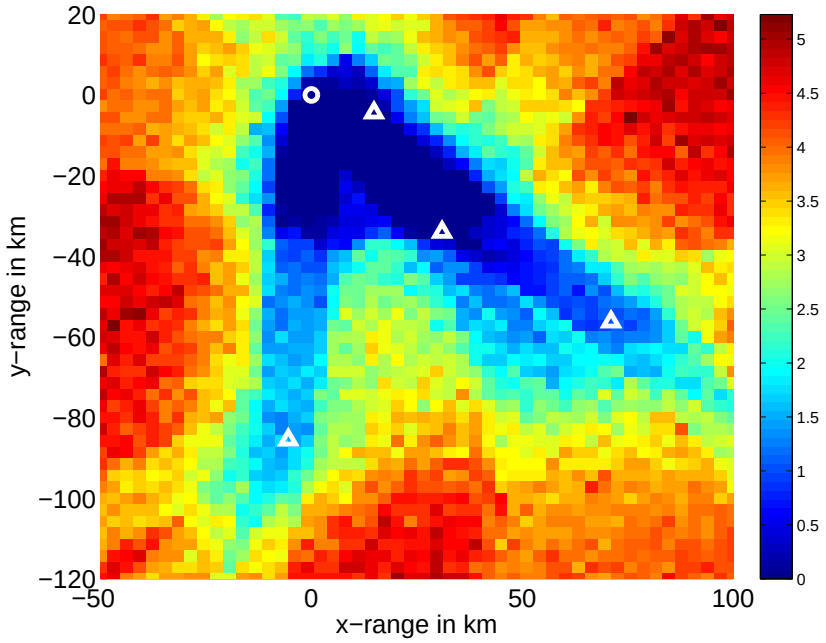

Figure 11: Scenario with 4 illuminators (shown by triangles) and one receiver (circle). Color bar denotes the mean number of probable estimates belonging to the true target.

4.1.1 Range dependence of the clutter Doppler

In monostatic sidelooking radar the look direction coincides with curves of constant Doppler (isodops). Both the look directions and the isodops are hyperbolas on the ground. This means that the clutter Doppler is range-independent. For any other configuration (monostatic forward looking, bistatic) the clutter Doppler depends generally on range. In Fig. 12 we find for illustration a bistatic along-track configuration with both the receiver (R) and the Transmitter (T) flying on the same path at the same speed. The black curves and colors are curves of constant clutter Doppler. The white hyperbolas denote the directions illuminated by the transmitter, i.e., those directions from where the ground echoes are scattered back. As this configuration is close to monostatic the isodops look similar to hyperbolas, however slightly different from the transmit directions which is an indication for a slight range dependence of the clutter Doppler. The range dependence can be seen clearly in the azimuth-Doppler contour plot (Fig. 13). For large ranges the contour becomes a diagonal which is the azimuth-Doppler curve of sidelooking monostatic radar. In this case the clutter echoes are range independent. Fig. 14 shows the associated STAP processor performance (improvement factor vs normalized Doppler, look direction 80). It can be noticed that the Doppler position clutter notch (i.e. the region where detection is unlikely) varies with range.

In Fig. 15 the transmitter flight direction has been chosen orthogonal to the receiver. As can be seen this causes a dramatic distortion of the isodops. Fig. 5 shows the associated azimuth-Doppler contour plot. Again we notice the range dependence of the clutter Doppler. Adaptation of the STAP processor requires the estimation of the space-time clutter covariance matrix from secondary data (clutter data from neighbouring range cells.). This is possible only if the clutter Doppler is constant with range. If not (as in the examples shown) certain techniques for Doppler compensation [5,6], azimuth-Doppler compensation [28] and alignment of the azimuth-Doppler contours have to be applied to the secondary data before estimation of the clutter covariance matrix.

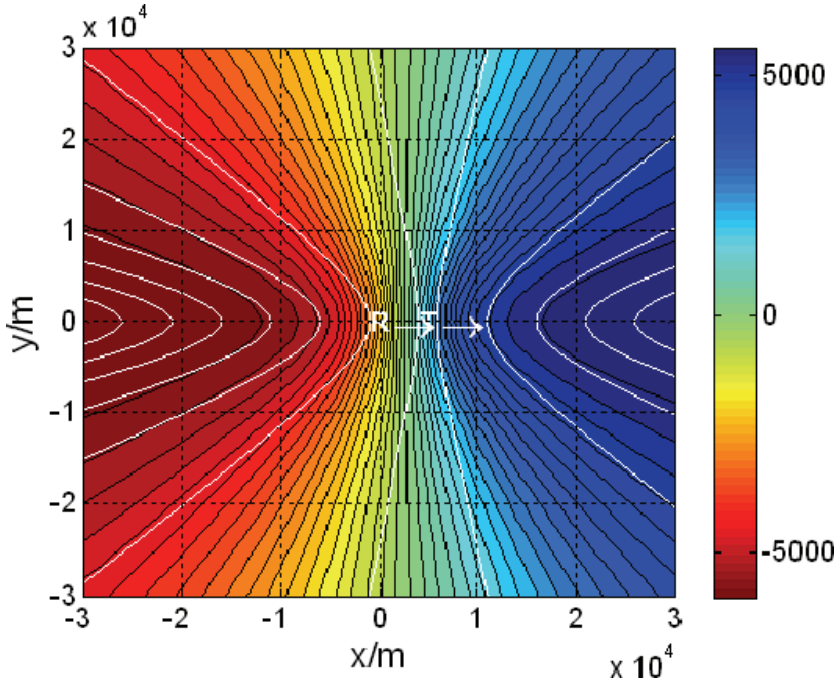

Figure 12: Isodops for bistatic airborne radar, horizontal along track configuration, R and T aligned, $\nu_R = \nu_T = 90$ m/s, platform height: 5000m, color bar denotes Doppler [Hz].

4.1.2 Doppler distribution on the ground

In Fig. 12 the distribution of clutter Doppler frequencies is fairly homogeneous. i.e., the spatial Doppler gradient is relatively constant. Exceptions can be noticed in and against the flight direction where larger areas with nearly constant Doppler can be noticed. However, a sidelooking antenna will be blind in these directions (nulls of element patterns) so that the constant Doppler areas have no significant effect on the detection performance during tracking. It should be remarked that in forward looking monostatic radar the large constant Doppler areas show up right in the main look direction which may be exploited to simplify the STAP architecture. If receiver and transmitter move on different paths (Fig. 4) the large constant Doppler areas may move to angles visible by the radar, here the lower left (dark red) and upper right (dark blue) corners. Under such conditions the constant Doppler areas will have impact on the tracking process. If the tracked target moves through such a constant Doppler area at the clutter Doppler frequency, much wider clutter notches (areas of low probability of detection) may be observed during tracking than determined by the system dimensions (array aperture, coherent processing interval; such notches can be seen in Fig. 14). It should be noted that configurations as shown in Fig. 15 are divergent, i.e., the configuration and hence, the bistatic radar properties change with time. In addition to the widening of clutter notches during tracking the variability of the bistatic configuration causes additional complexity. Certainly constant configurations as shown in Fig. 1 (others are possible) are easier to handle and avoid wide clutter notches. However, in some applications such as hybrid bistatic space/air configurations variable configurations are unavoidable because the flight path of the space based transmitter is predetermined by the satellite and the flight path of the receiver is determined by the mission.

4.2 Elements of Bayesian GMTI tracking

In a Bayesian view, track maintenance is an iterative updating of conditional probability densities of the (joint) kinematical target state $\mathbf{x}_k$ at time t_k given all accumulated sensor data Z^k and all available a priori information on the target dynamics and the sensor performance in terms of statistical models. Each update

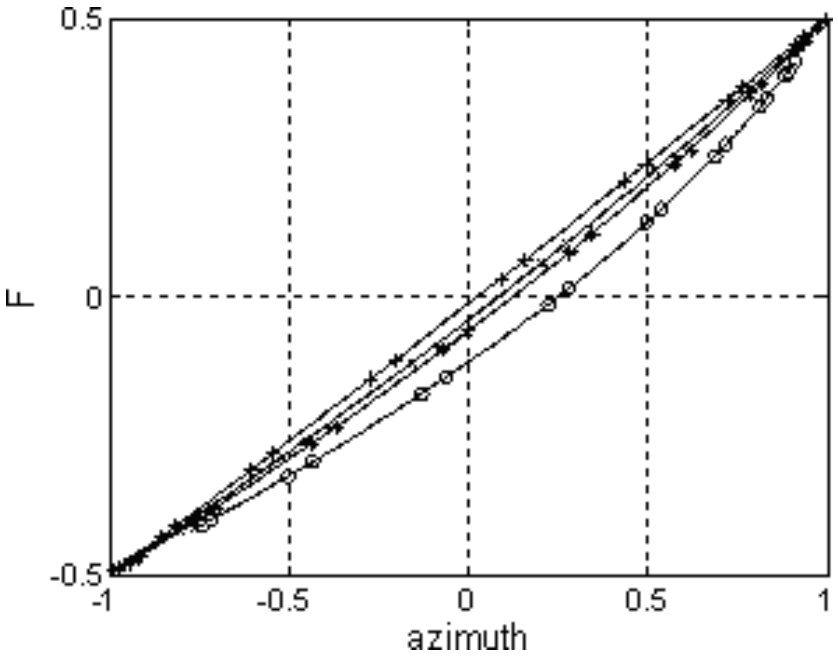

Figure 13: Doppler-azimuth contours for the configuration in Fig. 1 (normalized Doppler vs cosine of azimuth angle, o R=10km, * R=20km, x R=30km, + R=100km)

consists of a prediction, which is determined by the target dynamics model. The prediction is followed by a filtering step, which exploits the current sensor data and the sensor model. The sensor data at each scan k, as well as the sensor model, are the constituents of the likelihood function. According to Bayes' rule the conditional density at time k given all sensor data up to and including time k can be calculated from the prediction and the likelihood function. In many cases the sensor data are ambiguous; i.e. there exists a set of exhaustive and mutually exclusive data interpretations. We thus have to deal with densities obeying the structure of finite mixtures, weighted sums of individual densities. This is a consequence of ambiguities inherent in the data or the models used. From the densities optimal estimators can be derived according to particular cost functions.

4.2.1 System Model

The target state $\mathbf{x}_k = (\mathbf{p}_k, \mathbf{v}_k)^T = (x_k, y_k, z_k, \dot{x}_k, \dot{y}_k, \dot{z}_k)^T$ is given in 3D Cartesian coordinates assuming a linear movement model. In the same way the localization and velocity of the source and reveiver is given by $\mathbf{x}_k^S = (x_k^S, y_k^S, z_k^S, \dot{x}_k^S, \dot{y}_k^S, \dot{z}_k^S)^T$ and $\mathbf{x}_k^R = (x_k^R, y_k^R, z_k^R, \dot{x}_k^R, \dot{y}_k^R, \dot{z}_k^R)^T$. Here we consider measurements in terms of the bistatic range r_k, the azimuth φ_k, the elevation ϑ_k and the bistatic range-rate $\dot{r}_k$, which is proportional to the measured Doppler shift. The measurement equation $\mathbf{z}_k = (r_k, \varphi_k, \vartheta_k, \dot{r}_k)^T = h(\mathbf{x}_k)$is given by:

$$
\begin{aligned}
r_k &= ||\mathbf{p}_k - \mathbf{p}_k^S|| + ||\mathbf{p}_k - \mathbf{p}_k^R|| \\
\varphi_k &= \arctan \frac{y_k - y_k^R}{x_k - x_k^R} \\
\vartheta_k &= \arctan \frac{z_k - z_k^R}{\sqrt{(x_k - x_k^R)^2 + (y_k - y_k^R)^2}} \\
\dot{r}_k &= \frac{(\mathbf{p}_k - \mathbf{p}_k^S)(\mathbf{v}_k - \mathbf{v}_k^S)^T}{||\mathbf{p}_k - \mathbf{p}_k^S||} + \frac{(\mathbf{p}_k - \mathbf{p}_k^R)(\mathbf{v}_k - \mathbf{v}_k^R)^T}{||\mathbf{p}_k - \mathbf{p}_k^R||}
\end{aligned}
\tag{29}
$$

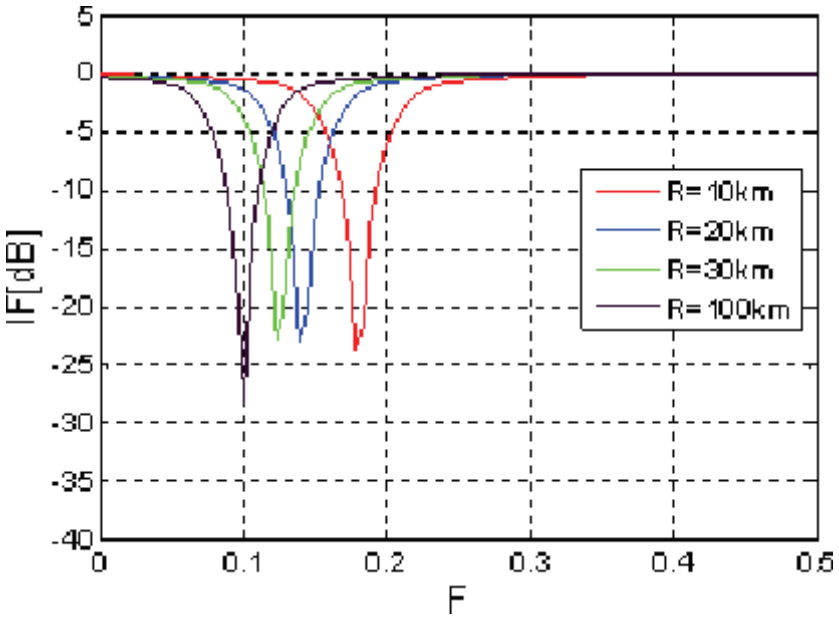

Figure 14: Improvement factor vs normalised Doppler: range dependence of clutter notches /look direction 80)

Assuming the target to be constantly moving at height zero the approach can also be applied to measurements of the bistatic range, the azimuth and the bistatic range-rate only.

4.2.2 Track Initialization

The measurement equation described above is everything we need to apply the Unscented Kalman Filter update formulas [8]. However, for track initialization in 3D Cartesian we need to transform measurements into the Cartesian space. Again we use Unscented Transform to generate an initial estimate in x,y and z. The transformation can be determined analytically, but is too lengthy to be displayed here (we used MATHEMATICA [33] to solve the equations).

4.2.3 GMTI-specific likelihood function

Doppler blindness occurs if the bistatic radial velocities of the target as well as the velocity of the surrounding mainlobe clutter return are nearly identical. This defines the location of the bistatic GMTI clutter notch in the state space of a ground target and, as such, reflects a fundamental physical fact without implying any further modeling assumptions. The detection model must thus reflect the following phenomena:

(i) The detection probability depends on the target state and the sensor/ target geometry,

(ii) The detection probability is small in a certain region around the clutter notch characterized by the minimum detection probability (MDV),

(iii) far from the clutter notch, the detection probability depends only on the directivity pattern of the sensor and the target,

(iv) there is a narrow transient region.

In this work we will only analyze the effect of the clutter notch, so the probability of detection is modeled to be fixed outside of the clutter notch, its value is given by p_D. Let $\dot{r}_t$ be the range-rate of the target and $\dot{r}_C$

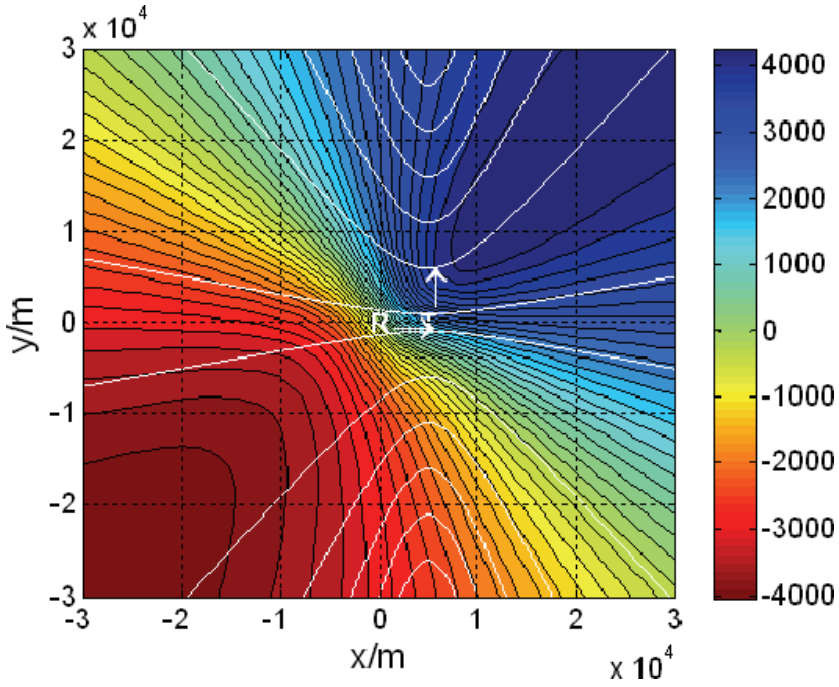

Figure 15: Isodops for bistatic airborne radar, orthogonal flight directions of R and T, $\nu_R = \nu_T = 90$m/s, platform height: 5000m, color bar denotes Doppler [Hz].

the range-rate of the corresponding background, then we consider the distance $n_c(\mathbf{x}_k) = |\dot{r}_t - \dot{r}_C|$. In close analogy to the discussion in [1,9] the detection probability can be written as a sum of Gaussian-type functions reflecting the current sensor-to-target geometry which describes the basic underlying physical facts.

$$P_D(\mathbf{x}_k) = p_D \left(1 - \frac{MDV}{\sqrt{\ln(2)/\pi}} \mathcal{N}\left(0; n_C(\mathbf{x}_k), \frac{MDV^2}{2\ln(2)}\right)\right) \tag{30}$$

'Negative' sensor evidence [32], i.e. the lack of an expected sensor measurement, is equivalent to a fictitious measurement (here: the distance between two range-rates is zero), which provides some information.

Provided detection has actually occurred, the measurements of the kinematical target parameters bistatic range, azimuth, elevation and bistatic range-rate are assumed to be bias-free with normally distributed measurement errors. As is usual in the tracking literature, false detections or detections produced by unwanted objects are assumed to be equally distributed in the measurement space and independent from revisit to revisit, their number being Poisson distributed with a spatial false return density ρ_F. For a set of incoming measurements $\mathbf{Z}_k = (\mathbf{z}_k^1, \mathbf{z}_k^2, \cdots, \mathbf{z}_k^{n_k})$ the following interpretation possibilities exist

1. One of the n_k measurements belongs to the target
2. One of the n_k measurements belongs to the target, even through the target is near to the Clutter Noch
3. The target has not been detected since it is in the Clutter Notch.
4. The target has not been detected due to other reasons $(1 - p_D)$.

The tracking update is driven by the likelihood function which proves to be proportional to a sum of Gaussians. Let $G_f = \mathcal{N}\left(0; n_C(\mathbf{x}_k), \frac{MDV^2}{2\ln(2)}\right)$ be the Gaussian density w.r.t. the fictitious measurement and

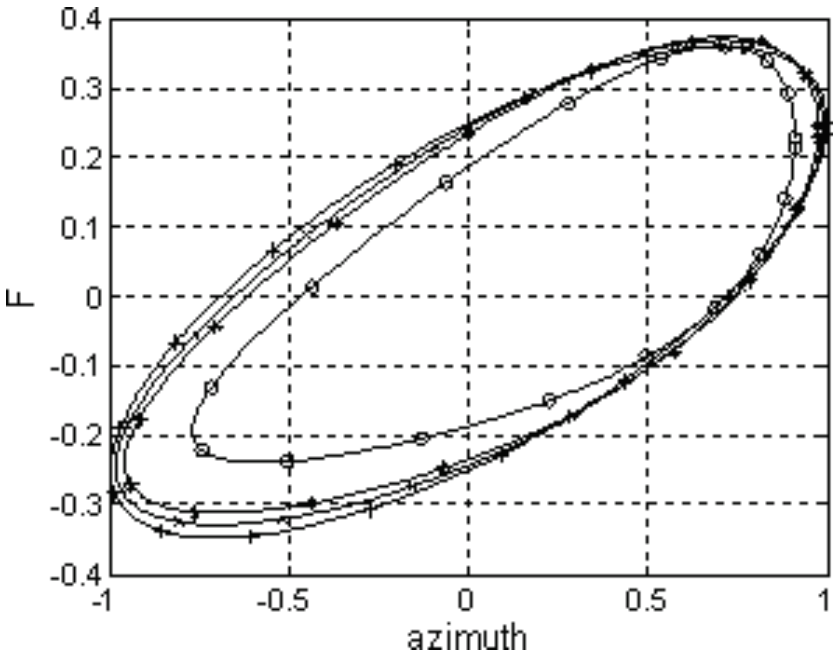

Figure 16: Doppler-azimuth contours for the configuration in Fig. 4 (normalised Doppler vs cosine of azimuth angle, o R=10km, * R=20km, x R=30km, + R=100km)

$G_m^n = \mathcal{N}(\mathbf{z}_k^n, h(\mathbf{x}_k), \mathbf{R})$ then

$$\begin{aligned} & p(\mathbf{Z}_k, n_k|\mathbf{x}_k) \\ & \propto (1 - P_D(\mathbf{x}_k))\rho_F + P_D(\mathbf{x}_k) \sum_{n=1}^{n_k} G_m^n \\ & = (1 - p_D)\rho_F + p_D\rho_F \frac{MDV}{\sqrt{\ln(2)/\pi}} G_f \\ & + \sum_{n=1}^{n_k} \left(p_D G_m^n - p_D \frac{MDV}{\sqrt{\ln(2)/\pi}} G_m^n G_f \right) \end{aligned} \tag{31}$$

Form this and the predicted density $p(\mathbf{x}_k|Z^{k-1})$ we can deduce the updated density by

$$p(\mathbf{x}_k|Z^k) \propto p(\mathbf{Z}_k, n_k|\mathbf{x}_k) p(\mathbf{x}_k|Z^{k-1}). \tag{32}$$

The derivation of the update formulas leads to the standard Kalman update formulas by using the fictitious measurement in the cases 2 and 3 [22],[30]. Conditional probability densities of the target state prove to be a Gaussian mixture in an approximate sense. We have to be aware of possibly negative mixture coefficients. This reflects the fact that, in case of detection, the target must have a certain minimum distance from the clutter notch, otherwise it could not have been detected at all. Nevertheless, also the possibly negative coefficients sum up to one.

Fusion of Information from Different Bistatic Geometries Availability of more than one source or receiver will result in additional detection opportunities. If the measurements of n_S bistatic geometries are gathered synchronously the cumulative probability of detection P_D^c can be written as

$$P_D^c = 1 - \prod_{i=1}^{n_S} (1 - P_D^i), \tag{33}$$

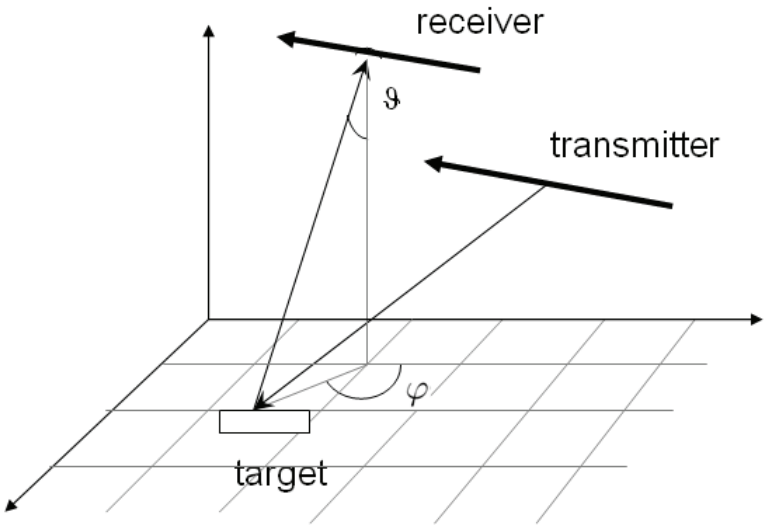

Figure 17: Bistatic geometry; two flying platforms (transmitter and receiver); and one ground moving target

where P_D^i denotes the probability of the ith source-receiver geometry. In section 4.3 we will present results of a multistatic geometry concerning one source and two receivers. The bistatic approach can be easily expanded, by updating the target state at time t_k for both geometries after each other.

Realization aspects To control the number of mixture components we follow the spirit of the standard PDA approach. At each time the Gaussian mixture will be approximated by a single Gaussian. The generalization to more refined approximation techniques is straightforward and leads to MHT (multiple hypothesis tracking).

4.3 Tracking Results: Discussion

In this section selected numerical examples are discussed based on the notional set of radar parameters. We consider the following scenario, see Fig. 18: Three flying sensor platforms, one source and two receivers are moving in different heights but with same speed, $\dot{x}^R = \dot{x}^T = 110$ m/s. The ground moving target drives diagonal to the path of the sensors with velocity of 5m/s in x and y direction. The duration of the simulation is 500seconds with sampling rate of 5seconds. In second 360 the target stops for 80 seconds. First we look at the two possible bistatic geometries, concerning receiver$_1$ and receiver$_2$ separately. For both cases the target is in a geometrical Clutter Notch as can be seen by calculating the expected probability of detection (P_D) according to the modeling assumptions, see Fig. 19. For receiver$_1$ the P_D is quite low during the most of the run. With respect to receiver$_2$ it starts with a better P_D but as an additional challenge the target stop event occurs for the same time at which the target is also in the geometrical clutter notch. Figures 20 and 21 illustrate the tracking performance in terms of the root mean squared error (RMSE) and the tracking error variance as a function of time (Cartesian position in ground coordinates and velocity in x/y). In the figures the impact of the GMTI clutter notch model on the tracking performance is compared with the standard approach, which ignores the detection model. Each performance measure has been calculated in a Monte-Carlo simulation over 100 runs. The deviations of the measurement errors in the simulation and as parameters of the tracking algorithm has been set to $(\sigma_r, \sigma_\varphi, \sigma_\vartheta, \sigma_{\dot{r}}) = (50\text{m}, 0.1^o, 1^o, 6.6\text{m/s})$ for the bistatic range, the azimuth, the elevation and of the bistatic range-rate. The shadowed region indicates the square-root of the corresponding diagonal element in the covariance matrix provided by the tracking filter. It is a measure for the "self consciousness" of the tracking filter. For both cases we observe improved estimation errors and a slight decrease in the corresponding estimation error covariance by using the clutter

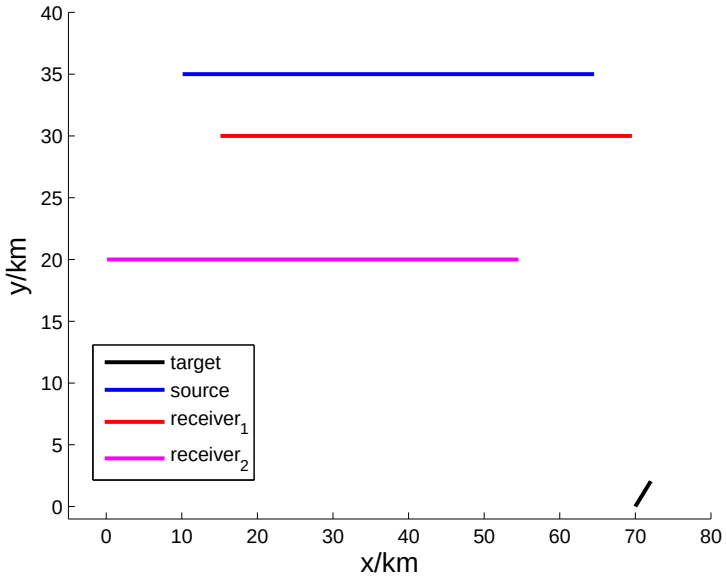

Figure 18: Considered multistatic scenario; two receiver one source; one ground moving target

notch model. Even though a track is initiated by a true measurement a low probability of detection and the consideration of false measurements may cause that for some tracks the estimated target state $\mathbf{x}_{k|k}$ differs strongly from the true trajectory $\mathbf{x}_k$. Let $P_{k|k}$ be the estimated covariance for time k, then we will mark tracks as "death" if $||\mathbf{x}_{k|k} - \mathbf{x}_k|| > 4\sqrt{\max(\text{eig}(\mathbf{P}_{k|k}))}$ and exclude them from the error statistics. The number of "death" tracks for the tracking concerning receiver$_1$ is 25% (clutter notch model) and 56% (without clutter notch modell), as well as 18% (clutter notch Model) and 50% (no clutter notch Model) for receiver$_2$. So, imbedding the clutter notch model in the tracking algorithm provides some opportunities to hold track in spite of bad tracking conditions. Finally, by fusing the information of the two bistatic geometries, Fig. 22, the estimation performance improves and the target stopping event is clearly detected by the clutter notch model. Due to the improved total probability of detection the number of death tracks has decreased to 0% for the clutter notch model and 5% else.

5 Conclusion

- We provided a multi-stage MHT algorithm, adapted on the special request of using DAB or DVB-T. The key challenge on target tracking in these single frequency networks is, that the association between illuminator and measurements is unknown. We demonstrated this aspect by means of simulation and developed a strategy to evaluate association possibilities by using sequential LR testing.

- We included numerical analysis using one hundred Monte Carlo runs for all three tracking stages. Especially, improvements in estimation performance by combining multiple measurement information has been pointed out.

- The algorithm is still in development and its potential is not yet exploited. The strength of the algorithm lies in dividing the whole procedure in partial stages. Information transfer between these stages has to be handled carefully and needs to be optimized to make the algorithm to work as good as possible. For example an improved transfer from the 3D-Tracking to 2D-Tracking should make the algorithm more robust and precise.

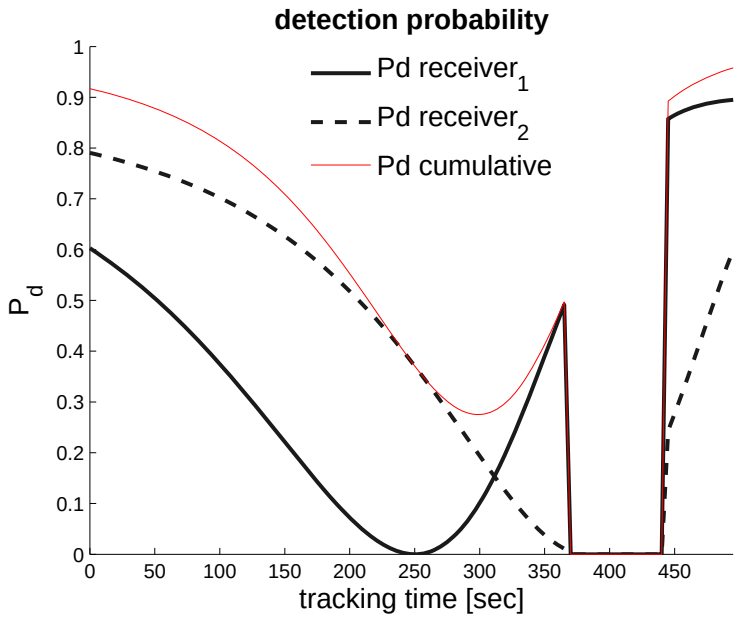

Figure 19: Probability of detection for the considered scenario; calculated according to the modeling assumptions

- In bistatic air-to-ground applications in general the bistatic clutter Doppler is range dependent.
- The isodop charts show in general areas of high and low Doppler gradient. For sidelooking monostatic radar constant Doppler areas coincide mostly with the nulls of the array element patterns and have no significant impact on the tracking process.
- For other configurations (transmit and receive paths with different directions, forward looking) large areas of constant Doppler may occur at angles visible by the radar which may lead to wide clutter notches during tracking.

With respect to the tracking performance bistatic air-to-ground applications we made the following observations from our numerical investigations:

- By exploiting the proposed bistatic GMTI detection model in combination with approximations of the type used in Unscented Kalman filtering in the tracking process we obtain a filter performance which is more or less consistent in that the RMS error of the tracker is nearly the same as the filter covariance for the multistatic approach and slightly pessimistic in bistatics.
- In case of a target-in-clutter-notch-event the filter error covariances are reduced in size if the clutter notch model is used. This has impact on all decisions based to the tack innovation statistics in a tracking system.
- The target-stop-event itself can be detected and especially in the multistatic scenario it is characterized by a very low RMSE error with respect to target velocity. This has impact on track continuity, an important performance measure in system applications.
- Even in case of a poor detection performance a certain track quality can still be obtained provided the proposed bistatic GMTI detection model is used.

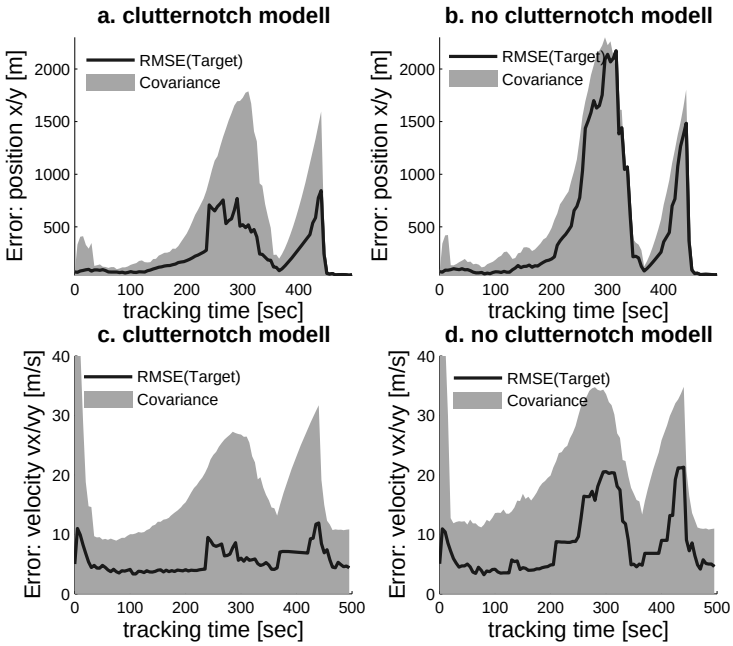

Figure 20: Estimation performance for bistatic geometry concerning receiver$_1$; results for the clutter notch model (left) is compared to the standard tracking result (right)

References

[1] P. Howland, D. Maksimiuk, and G. Reitsma, FM radio based bistatic radar, Radar, Sonar and Navigation, IEE Proceedings-, vol. 152, no. 3, pp. 107115, June 2005.

[2] M. Tobias and A. Lanterman, Probability hypothesis density-based multitarget tracking with bistatic range and doppler observations, Radar, Sonar and Navigation, IEE Proceedings-, vol. 152, no. 3, pp. 195205, June 2005.

[3] U. Reimers, Digitale Fernsehtechnik. Springer, 1995.

[4] N. J. Willis, Bistatic Radar. SciTech Publishing, 2007.

[5] W. Koch, J. Koller, and M. Ulmke, Ground target tracking and road map extraction, ISPRS Journal of Photogrammetry & Remote Sensing, vol. 61, p. 197 208, 2006.

[6] M. Daun and C. R. Berger, Track initiation in a multistatic DAB/DVB-T network, submitted for FUSION Conference, 2008.

[7] D. J. Torrieri, Statistical theory of passive location systems, IEEE Transactions on Aerospace and Electronic Systems, no. 2, pp. 183198, Mar. 1984.

[8] S. J. Julier and J. K. Uhlmann, "Unscented Filtering and Nonlinear Estimation," *Proceeding of the IEEE*, vol. 92, no. 3, 2004.

[9] O. E. Drummond. Target Tracking with Retrodicted Discrete Probabilities. In *SPIE **3163**, Signal and Data Processing of Small Targets*, 249 (1997).

[10] O. E. Drummond. Multiple Sensor Tracking with Multiple Frame, Probabilistic Data Association. In *SPIE **2561**, Signal and Data Processing of Small Targets*, 322 (1995).

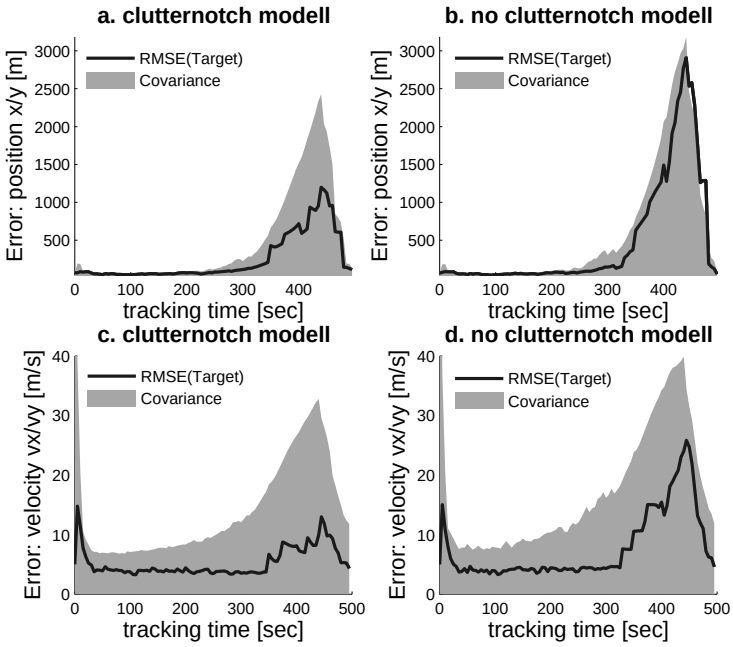

Figure 21: Estimation performance for bistatic geometry concerning receiver$_2$; results for the clutter notch model (left) is compared to the standard tracking result (right)

[11] O. E. Drummond. Multiple Target Tracking with Multiple Frame, Probabilistic Data Association. In *SPIE **1954**, Signal and Data Processing of Small Targets*, 394 (1993).

[12] A. Gelb (Ed.). *Applied Optimal Estimation*, MIT Press (1974).

[13] Martin E. Liggins, David L. Hall, and James Llinas (Eds.). *Handbook of Multisensor Data Fusion – Theory and Practice*. CRC Press, 2nd Edition (2008).

[14] D.M. Titterington, A.F.M. Smith, and U.E. Makov: *Statistical Analysis of Finite Mixture Distributions*, John Wiley & Sons (1985).

[15] D. L. Alspach and H. W. Sorenson, "Nonlinear Bayesian estimation using gaussian sum approximation". In *IEEE Transactions on Automatic Control*, Vol. 20, pp. 439447, 1972.

[16] M. Ulmke, O. Erdinc, and P. Willett. "Ground Moving Target Tracking with Cardinalized Gaussian Mixture PHD Filtering". In *Proc. of the 10th International Conference on Information Fusion FUSION 2007*, Quebec, Canada, July (2007).

[17] Christian R. Berger, Martina Daun, and Wolfgang Koch. "Low Complexity Track Initialization from a Small Set of Non-Invertible Measurements". In *EURASIP Journal on Advances in Signal Processing*, special issue on track-before-detect techniques, Vol. 2008, Article ID 756414, 15 pages, doi:10.1155/2008/756414 (2008).

[18] Ch. Berger, M. Daun, W. Koch. "Track Initialization from Incomplete Measurements". In *Proc. of 10th ISIF International Conference on Information Fusion*, Quebec, Canada, 2007.

[19] G. van Keuk. "Sequential Track Extraction". In *IEEE Transactions on Aerospace and Electronic Systems*, Vol. 34, pp. 1135 (1998).

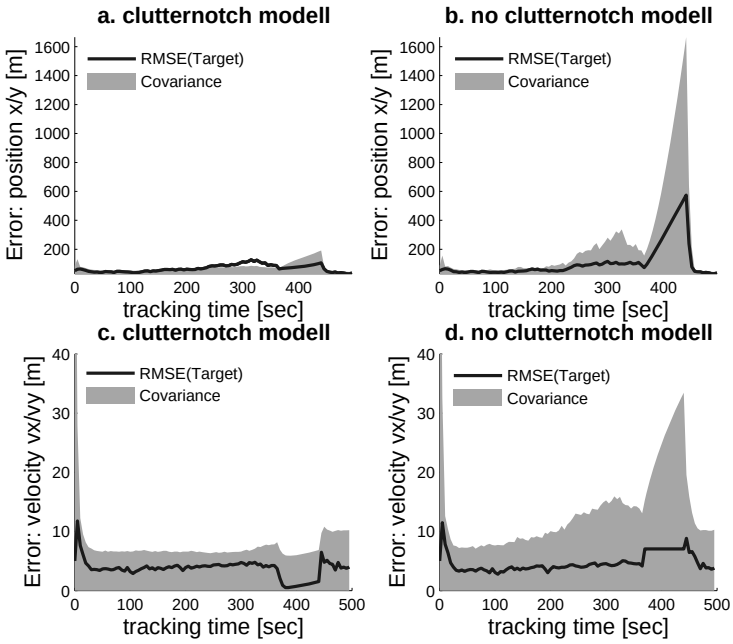

Figure 22: Estimation performance for fusing information of two bistatic geometries; results for the clutter notch model (left) is compared to the standard tracking result (right)

[20] Y. Boers and Hans Driessen. “A Particle Filter Multi Target Track Before Detect Application”. In *IEE Proceedings on Radar, Sonar, Navigation*, vol. 151, no. 6, 2004.

[21] M. Wieneke, W. Koch. “On Sequential Track Extraction within the PMHT Framework”, In *EURASIP Journal on Advances in Signal Processing*, Volume 2008, Article ID 276914, 13 pages, doi:10.1155/2008/276914 (2008).

[22] W. Koch and R. Klemm, “Ground target tracking with STAP radar”, *IEE Proc. Radar, Sonar and Navigation*, Vol. 148/3, June 2001, pp.173-185

[23] R. Klemm, U. Nickel and W. Koch, ”Single ground target tracking with adaptive monopulse radar. Pt. I: The sensor”, *EUSAR 2006*, 16-18 May 2006, Dresden

[24] W. Koch, R. Klemm and U. NICKEL, ”Single ground target tracking with adaptive monopulse radar. Pt. II: The tracker”, *EUSAR 2006*, 16-18 May 2006, Dresden

[25] R. Klemm, ”Principles of Space-Time Adaptive Processing”, *3rd ed. IET Publishers*, 2006, London

[26] G. K. Borsari, ”Mitigating effects on STAP processing caused by an inclined array”, IEEE RADAR-CON’98, 11-14 May 1998, Dallas, TX, pp. 135-140

[27] O. Kreyenkamp and R. Klemm, ”Doppler compensation in forward looking STAP radar”, *IEE Proc. Radar, Sonar and Navigation*, 2001, pp. 253-258

[28] B. Himed, ”Effects of bistatic clutter dispersion on STAP systems”, *IEE radar 2002*, 15-17 October 2002, Edinburgh, Scotland, pp. 360-364

[29] F. D. Lapierre, J. G. Verly and M. van Droogenbroek, ”New solutions to the problem of range dependence in bistatic STAP radars”, *IEEE Radar Conference*, May 5-8, 2003, Huntsville, AL, pp. 452-459

[30] W. Koch, ”Ground Moving Target Tracking with STAP Radar”, Chapter 14 in: Klemm, R., ed.: *Applications of space-time adaptive processing*, IEE Publishers, 2004.

[31] M. Daun and W. Koch, ”Multistatic Target Tracking for Non-Cooperative Illuminating by DAB/DVB-T”. *submitted for IEEE Radar Conference*, Rome, Italy, May 2008.

[32] W. Koch, ”’Negative’ Information in Tracking and Sensor Data Fusion: Discussion of Selected Examples”, *Proc. FUSION 2004*, pp. 91-98.

[33] Wolfram Research, Inc., ”Mathematica”, Version 5.2,*Wolfram Research, Inc.*, Champaign, Illinois,2005.